Differing regional responses to a perturbation in solar cloud absorption in the SKYHI general circulation model

Carynelisa Erlick,[1] V. Ramaswamy,[2] and Lynn M. Russell[3]

Received 13 July 2005; revised 22 October 2005; accepted 23 November 2005; published 22 March 2006.

[1] In this study we perform an idealized experiment to investigate the effect of solar absorption in clouds on climate using a general circulation model with prescribed sea surface temperatures, focusing on the manner of regional changes during the northern summer season. The response arising from this type of perturbation is akin to "semidirect" effects of absorbing aerosols, namely, dissipation of clouds owing to a high aerosol absorption in the cloud layers. In the experiment, we apply a similar perturbation to all low-cloud layers, reducing their single-scattering albedo to a value of 0.99, which enables us to isolate the effect of such solar absorption from other aerosol related influences. We find that in both midlatitude and equatorial regions, the reduction in low-cloud single-scattering albedo causes a reduction in low-cloud amount and a warming of the surface. However, the dynamical response of the system varies from one continental region to another. In the midlatitude regions of the United States and Europe/east Asia, the diabatic heating perturbation leads to the dissipation of low clouds, an increase in shortwave flux to the surface, an increase in horizontal heat advection, and an increase in atmospheric stability. In the tropical region of North Africa, the diabatic heating perturbation translates into an increase in convection, a decrease in stability, an increase in middle- and high-level clouds, and a reduction in shortwave flux to the surface. In agreement with previous studies, these results demonstrate the distinctive response of the tropical versus midlatitude regions to a similar solar perturbation.

Citation: Erlick, C., V. Ramaswamy, and L. M. Russell (2006), Differing regional responses to a perturbation in solar cloud absorption in the SKYHI general circulation model, *J. Geophys. Res.*, *111*, D06204, doi:10.1029/2005JD006491.

1. Introduction

[2] A number of recent investigations have shown that aerosol particles can have competing effects on cloud microphysical and radiative properties, depending on their own microphysical and radiative characteristics. Under the heading of indirect effects, increases in absorbing and nonabsorbing aerosols have been shown to increase cloud drop concentration and cloud reflectivity [*Twomey*, 1991; *Pincus and Baker*, 1994; *Lohmann et al.*, 2000], reduce precipitation efficiency [*Rosenfeld*, 1999, 2000], and increase cloud lifetime [*Albrecht*, 1989]. Under the heading of semidirect effects, or more broadly speaking under the heading of aerosol-cloud interactions, increases of absorbing aerosols, such as soot and dust, have been shown to reduce cloud amount when they are present either in the interstitial air between cloud drops or within drops [*Ackerman and Toon*, 1996; *Hansen et al.*, 1997, 2000; *Ackerman et al.*, 2000; *Lohmann and Feichter*, 2001; *Conant et al.*, 2002; *Johnson et al.*, 2004; *Cook and Highwood*, 2004].

[3] On the basis of two Monterey Area Ship Track (MAST) experiment case studies, *Erlick et al.* [2001] found that absorbing aerosols from a continental air mass can decrease the visible single-scattering albedo (SSA) of clouds from near 1.0 to a lower bound of 0.994. (For the idealized experiment carried out here we increase the amount of absorption over 50% by using 0.99 instead.) Using a one dimensional radiative convective model (RCM), it was shown that in the absence of microphysical or cloud-climate feedbacks, the resulting increase in solar heating within the cloud layer causes a warming of the troposphere and surface, an increase in water vapor, and a stabilization of the atmosphere [*Erlick and Ramaswamy*, 2003]. With only low clouds perturbed, and no perturbation to the cloud optical depth, the calculated forcing due to this solar absorption in low clouds was 4.5 W m^{-2}, which is significant in comparison of estimated forcings due to anthropogenic greenhouse gases [*Ramaswamy et al.*, 2001].

[4] In this study, we extend the experiment of *Erlick and Ramaswamy* [2003] to allow microphysical and cloud-climate feedbacks within the context of GFDL's SKYHI general circulation model (GCM). Performing an idealized experiment, we apply a similar perturbation to all low-cloud layers, reducing their single-scattering albedo to 0.99, and look at the responses of different regions to this

[1]Department of Atmospheric Sciences, Hebrew University of Jerusalem, Jerusalem, Israel.
[2]Geophysical Fluid Dynamics Laboratory, Princeton University, Princeton, New Jersey, USA.
[3]Scripps Institution of Oceanography, University of California, San Diego, California, USA.

0148-0227/06/2005JD006491$09.00

perturbation. *Liousse et al.* [1996] and *Cooke et al.* [2002] have shown that carbonaceous aerosol absorption occurs in both the midlatitudes and tropical regions. *Hansen et al.* [1997] showed that aerosol induced increases in cloud absorption can produce a similar forcing in midlatitude and tropical regions, but that the regional response can comprise contrasting compensations. *Lofgren* [1995a, 1995b] and *Chen and Ramaswamy* [1995] likewise applied a solar forcing to midlatitude and tropical regions and found differing dynamical responses in the different regions. By perturbing all low clouds similarly, we are able to isolate the effect of solar absorption in clouds from other aerosol related influences and identify the mechanisms responsible for the differing dynamical responses. While many aspects of semidirect effects remain to be observed and studied, a modeling study such as this is required in order to flush out the processes that may be operating and to identify the mechanisms involved. In particular, we ask whether the nature of the response in all regions is identical. Do all continental regions undergo the same response to a similar perturbation to the low-cloud radiative properties, namely, perturbation of solar absorption by low-cloud layers?

2. Model Description

[5] A more complete description of the SKYHI GCM can be found in *Hamilton et al.* [1995] and *Schwarzkopf and Ramaswamy* [1999]; only a brief summary is included here. The model contains 40 vertical levels, with ~1 km resolution in the troposphere, ~2 km resolution in the stratosphere, and ~3 km resolution in the mesosphere extending up to 80 km altitude. The latitude-longitude resolution is $3.0° \times 3.6°$. Clouds are diagnosed, whereby a model layer in a certain grid box is given a cloud amount of 1.0 whenever the relative humidity reaches 100% [*Wetherald and Manabe*, 1988], while the relative humidity itself is prognostically determined owing to the fact that temperature and water vapor amount are prognostic variables in the model. (In the discussion of the results that follow, a change in "cloud amount" refers to a change in the spatially averaged frequency of occurrence of clouds [*Wetherald and Manabe*, 1988].) The simplicity of this cloud scheme allows for a relatively straightforward interpretation of the results under perturbation of the cloud properties. The radiative properties of the clouds that form are determined by the altitude of cloud, with low clouds defined to be those forming between 680 and 1000 hPa, middle clouds defined to be those forming between 440 and 680 hPa, and high clouds defined to be those forming between 10 and 440 hPa. Total extinction optical depths at 0.55 μm wavelength for the low, middle, and high clouds, are fixed at 12, 3, and 1, respectively, while the variation with wavelength and the other single-scattering parameters are determined from the *Slingo* [1989] parameterization assuming a drop effective radius of 10 μm. The *Slingo* [1989] parameterization gives a nominal single-scattering albedo at 0.55 μm of 0.999998. The shortwave and longwave radiation schemes in SKYHI are described by *Freidenreich and Ramaswamy* [1999], *Schwarzkopf and Fels* [1991], and *Schwarzkopf and Ramaswamy* [1999], respectively. This model has been successfully used to investigate the global climate effects of radiative perturbations [e.g., *Ramachandran et al.*, 2000; *Ramaswamy and Schwarzkopf*, 2002].

[6] In our simulations, the single-scattering albedo of low clouds only is reduced to 0.99 for wavelengths between 0.2 and 1.2 μm (frequency 8200–57,600 cm^{-1}), the wavelength range of the decreases in cloud single-scattering albedo computed by *Erlick et al.* [2001] as a result of the influence of a continental air mass. The optical depths of the clouds are left unperturbed. This is similar to the low clouds only perturbation with nominal cloud optical depths in the RCM of *Erlick and Ramaswamy* [2003], except that the cloud amount is allowed to vary with time in each grid box and horizontal dynamics also plays a part. Again for simplicity of interpretation, the model's sea surface temperatures (SSTs) are prescribed in a similar fashion to *Chen and Ramaswamy* [1995] (fixed from year to year, but seasonally varying within a specific year), so that in assessing the surface temperature response we focus on the land surfaces only.

[7] In the simulations, the control run is a 13-year extension (of which 12 years are analyzed) of a 29-year standard SKYHI control experiment, the extension being that no clouds are allowed to form in the lowest two model layers. This restriction on the lowest two model layers, similar to one applied to earlier versions of the National Center for Atmospheric Radiation (NCAR) Community Climate Model (CCM), was implemented in order to correct an oversupply of wet deposition in the model. Note that such a restriction does not imply that there are no low clouds, specifically stratocumulus type clouds, in the model. Low clouds do indeed form in the third and fourth model layers, the third model layer often still within the lowest two kilometers from the surface, depending on latitude. The model was shown to exhibit a realistic global albedo even with the restriction on clouds in the lowest two layers.

[8] The perturbation to the low-cloud single-scattering albedo is run for 6 model years (rather than 12 due to restricted computer time) using the restart conditions after a year of the extension of the control experiment. Because the removal of clouds from the lowest two layers was a minor tuning to a very long control run, one year of the extension with prescribed SSTs was sufficient for the model to reach a quasi-steady state before the perturbation to the low-cloud single-scattering albedo was additionally applied.

3. Results

[9] In a similar fashion to *Chen and Ramaswamy* [1995], we chose to analyze the summer months as a first step in our idealized experiment, since the northern latitude summer is known to be more quiescent. The other northern hemisphere seasons, particularly winter, are known to be more variable owing to more baroclinic instability and the propensity of storm tracks [see, e.g., *Peixoto and Oort*, 1992, section 7.2.3]. If a statistically significant response is not discerned in the summer months, then the perturbation is not likely to be manifested in the annual mean [*Chen and Ramaswamy*, 1995; *Peixoto and Oort*, 1992]. Figure 1 shows the shortwave (SW) forcing, defined as the instantaneous change in net solar flux at the top of the atmosphere (TOA, Figure 1a) and at the surface (SFC, Figure 1b), for July of the first analyzed year of the perturbation. (In actuality, the forcing is calculated as the change in net solar flux during a single

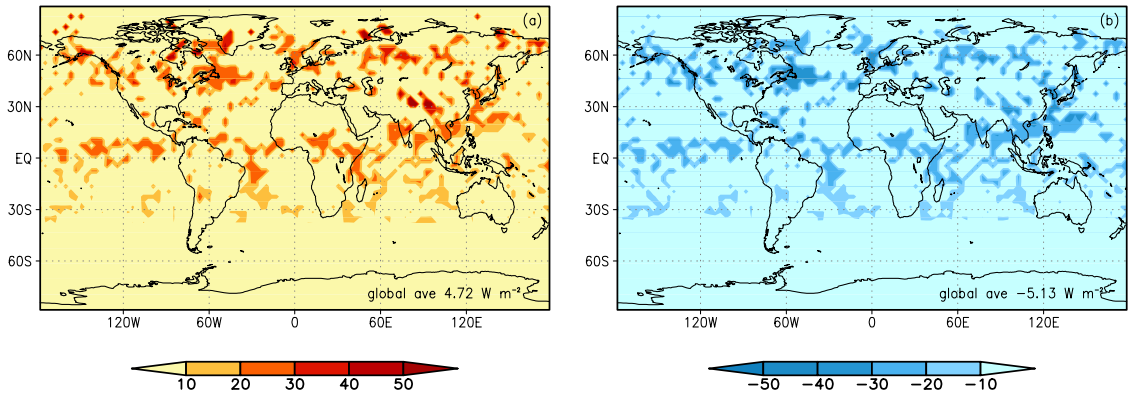

Figure 1. Shortwave forcing (W m^{-2}) for the month of July, defined as the instantaneous change in net shortwave flux (during a single radiation time step in mid-July with no diurnal cycle) (a) at the TOA and (b) at the SFC. Global mean values are indicated in the lower right corner of each plot.

4-hour radiation time step on July 18th of the first analyzed year of the perturbation with no diurnal variation; this forcing may include small changes to the cloud amount during the intermediate dynamical time steps). The global average is indicated in the bottom right corner of each plot. As one would expect, the additional absorption within the low-cloud layers decreases the upward flux at the TOA and the downward flux at the SFC, resulting in a positive forcing at the TOA and a negative forcing at the SFC. The forcing at the SFC is of slightly larger magnitude than that at the TOA. The pattern of the forcing matches the initial pattern of low-cloud amount on July 18th. This type of inhomogeneous forcing, in which the cloud single-scattering albedo is perturbed, is different from the inhomogeneous forcing applied by *Chung et al.* [2002] in their study of Indo-Asian haze. In the work by *Chung et al.* [2002], the forcing imposed at the SFC is on the order of 3 times the forcing at the TOA, as discussed further in section 4.

[10] Figure 2 shows the change in June/July/August (JJA) mean low-cloud amount (the cloud amount in the third model layer is used as a proxy for the low-cloud amount; Figure 2a) and land surface temperature (Figure 2b) resulting from the forcing displayed in Figure 1. (Recall that a change in cloud amount refers to a change in the frequency of occurrence of clouds.) From Figure 2a, it is clear that the overall global effect on low-cloud amount is a reduction, as the absorption of solar radiation by the low clouds causes local heating and dissipation, but there are also pockets of increase, such that the pattern of the response does not match the pattern of the forcing. From Figure 2b, the overall effect on land surface temperature is an increase, but likewise there also are pockets of decrease. On the whole, the land surface warms as a result of the dissipation of some of the low clouds, which allows more solar flux to reach the surface. Additionally, from RCM considerations, the heating within the low-cloud layers may be expected to lead to further warming of the surface via communication of heat to the surface. Note that globally, the outgoing longwave flux from the surface may increase; this is to be compared with the increase in the shortwave surface flux as a result of the low-cloud dissipation. Our results demonstrate that the increase in incoming shortwave is more dominant in determining the land surface temperature, hence yielding a warming. (See the discussion of Table 1 that follows.)

[11] The change in mean SW flux at the (1) TOA and (2) SFC resulting from the changes in cloud amount and other model variables is shown in Figure 3. Note that this is the equilibrium change in SW flux, as opposed to the forcing, or instantaneous change in SW flux, displayed in Figure 1. The global average values are again indicated in

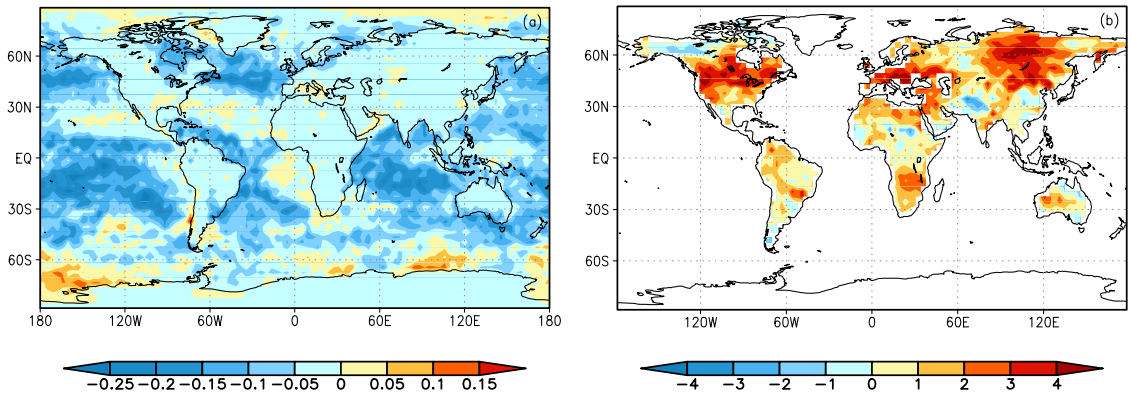

Figure 2. (a) Change in JJA mean low-cloud amount between the 6-year perturbation and the 12-year control. The cloud amount in the third layer (no clouds are allowed to form in the bottom two layers) is used as a proxy for total low-cloud amount. (b) Change in JJA mean land surface temperature (K).

Table 1. JJA Mean Change Between the 12-Year Control and the 6-Year Perturbation for the Global Mean and Three Separate Regions[a]

Quantity	Global Mean	United States (Land Only)	Europe/East Asia (Land Only)	North Africa (Land Only)
T SFC (land), K	1.2	2.3	2.2	0.7
SW TOA, W m^{-2}	12.6	11.3	9.3	4.0
LW TOA, W m^{-2}	−1.9	−3.3	−5.2	2.0
SW ATM, W m^{-2}	4.9	5.4	3.9	4.7
SW SFC, W m^{-2}	7.7	5.9	5.4	−0.7
LW SFC, W m^{-2}	−3.0	−0.7	−2.3	1.6
SH SFC, W m^{-2}	−1.0	3.4	5.2	−1.6
LH SFC, W m^{-2}	−4.5	1.4	−3.3	2.5
EVAP+SUBL, J	−0.02	0.004	−0.01	0.008
SOIL MOISTURE, cm	−0.1	−1.0	−0.6	0.07
RAIN+SNOW, mm d^{-1}	−0.02	−0.01	−0.01	0.03
TOTCLD	−0.0002	—	—	—
TOTCLD (land only)	−0.022	−0.03	−0.03	0.01
LOWCLD	−0.06	—	—	—
LOWCLD (land only)	−0.018	−0.02	−0.01	−0.003
PREC WATER, mm	0.6	3.3	2.4	1.9

[a]Low cloud SSA = 0.99. T SFC is surface temperature; SW is net shortwave flux (down minus up); LW is net longwave flux (down minus up); TOA is top of the atmosphere; SW ATM is shortwave radiation absorbed in the atmosphere; SFC is surface; SH is sensible heat flux (positive is upward, that is, loss from the surface); LH is latent heat flux (positive is upward, that is, loss from the surface); EVAP+SUBL is evaporation and sublimation; TOTCLD is total cloud amount; LOWCLD is low cloud amount; PREC WATER is precipitable water, defined as the height to which the total atmospheric water vapor contained in a vertical column would stand if condensed and collected in a vessel of unit cross-sectional area.

the bottom right corner of each plot. At the TOA, there is a stronger increase in net SW flux than there was in the instantaneous forcing (12.6 W m^{-2} in the global average response as compared to 4.7 W m^{-2} in the instantaneous global average), while at the same time some pockets of decrease in net SW flux appear. The stronger increase in global net SW flux results from the fact that not only do existing low clouds absorb solar radiation, reducing the upward flux, but there is also an overall decrease in cloud amount (in response to the local forcing as well because of changes in the large-scale circulation). This reduction in cloud amount may be considered a negative feedback on absorbed SW flux when considering the fact that the low clouds in which the perturbation is taking place are being dissipated, but then there is a positive feedback on the net all-sky SW flux, or on the nature of the perturbation itself, at the TOA [*Hansen et al.*, 1997; *Cook and Highwood*, 2004].

[12] At the SFC, the picture is more complicated. The overall effect has switched sign from that of the instantaneous forcing (from −5.1 W m^{-2} to 7.7 W m^{-2} in the global average response), although several pockets of a decrease in net SW flux remain. The change in sign is again due to the dissipation of the low clouds. In the forcing calculation (for which the low-cloud amount does not vary) there is a reduction in SW flux to the SFC, while in the global mean response the cloud dissipation allows an increase in flux to the SFC. The pockets of decrease in net SW flux that remain (where less SW flux reaches the SFC) loosely coincide with areas where low-cloud amount increases rather than decreases (refer to Figure 2a), that is, in the Southern Ocean region and over Antarctica, over land in the latitude belt around 30°N, and along the equator off the west coast of Africa. An exception is the region of northeast Africa, including the Sinai peninsula (discussed further below), which exhibits decreases in low-cloud amount along with decreases in net SW flux to the SFC.

[13] Table 1 shows the mean changes in various quantities between the perturbation and control for the months

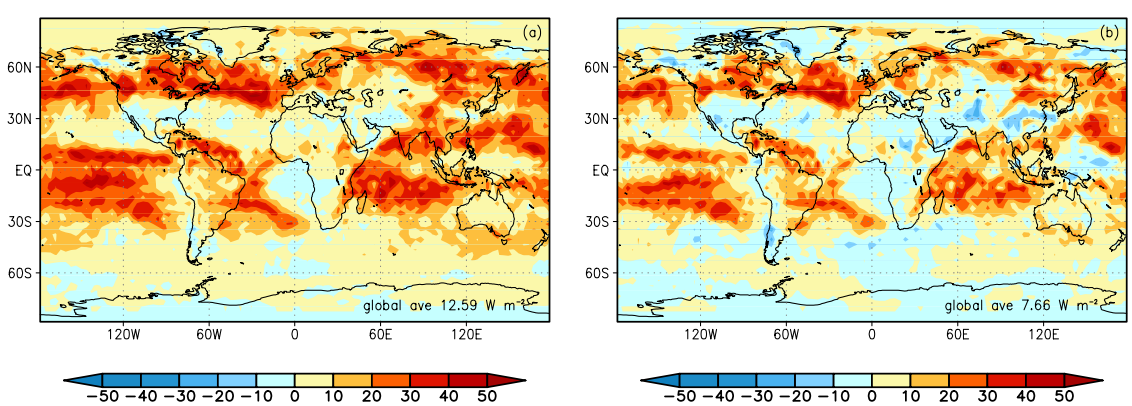

Figure 3. Change in JJA mean net shortwave flux (W m^{-2}) between the 6-year perturbation and the 12-year control (a) at the TOA and (b) at the SFC. Global mean values are indicated in the lower right corner of each plot.

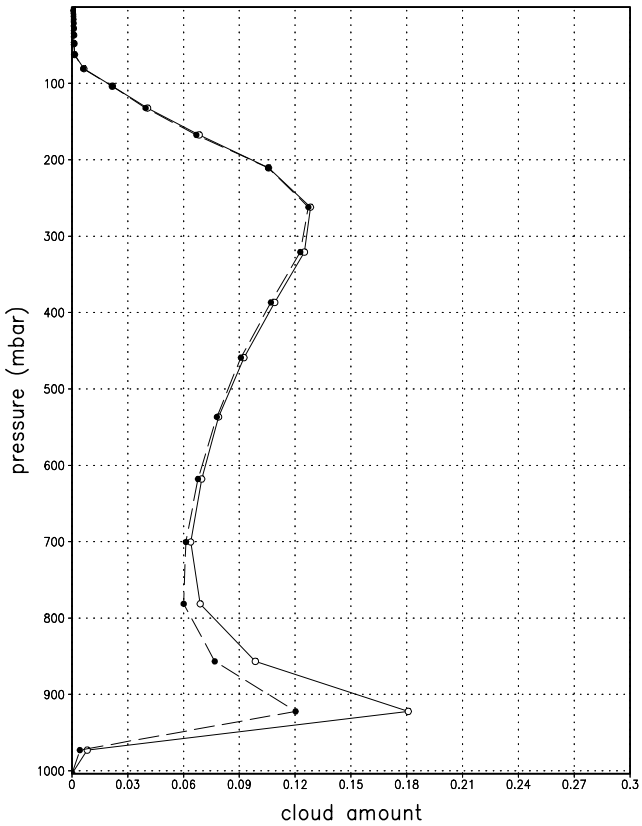

Figure 4. Global mean JJA mean cloud amount profile for the control (solid line) and the perturbation (dotted line).

June/July/August. The difference between the perturbation and control are shown for the global mean and for three separate land regions, United States (31.5°N–46.5°N, 135.0°W–52.2°W), Europe/east Asia (40.5°N–55.5°N, 12.6°W–88.2°E), and North Africa (7.5°N–28.5°N, 19.8°W–59.4°E).

[14] As is evident in Figures 2 and 3, in the global mean in JJA the low-cloud amount (LOWCLD) decreases, while the land surface temperature (T SFC) increases by 1.2 K, the net SW flux at the TOA (SW TOA) increases by 12.6 W m^{-2}, and the net SW flux at the SFC (SW SFC) increases by 7.7 W m^{-2}. The fact that the increase in SW flux at the TOA is larger than that at the SFC indicates that there is a net SW input to the atmosphere (of 4.9 W m^2 (SW ATM)), and as a result the system warms. In the global mean, the warmer atmosphere and surface together with the decrease in low clouds increases the upward longwave (LW) flux (decreases the LW flux into the system) by 1.9 W m^{-2} at the TOA and by 3.0 W m^{-2} at the SFC. The decrease in low-cloud amount is accompanied by a net decrease in total cloud amount (TOTCLD), which is also reflected in the JJA global mean vertical profile of cloud amount displayed in Figure 4. (Note that the global mean decrease in total cloud amount is smaller than the global mean decrease in low-cloud amount. This is due to a compensating effect of increasing middle- and high-cloud amount in the 0°N–30°N latitude band, as discussed further below with respect to the region of North Africa.)

[15] The altitude of cloud dissipation corresponds well with that of the SW heating increase (Figure 5). Like the RCM simulations of *Erlick and Ramaswamy* [2003], in the global mean there is a slight increase in water vapor (or precipitable water, PRECIP WATER) and an increase in atmospheric stability, which is reflected in the decrease in precipitation (RAIN+SNOW), soil moisture, evaporation and sublimation (EVAP+SUBL), and latent heat release from the surface (LH SFC). As in the RCM simulations, in the global mean the troposphere has warmed because of the input of SW flux, and the overall response is similar to that of the RCM, albeit with different physics considerations [*Erlick and Ramaswamy*, 2003]. However, this does not render an equivalence between RCM and GCM simulations for this kind of a perturbation. In the RCM, increased atmospheric stability results via consideration of radiative-convective processes, namely, diffusion of local cloud heating throughout the troposphere, with a slightly greater warming of the troposphere relative to the surface. In the GCM, the diabatic heating input via SW absorption does not translate into an increase in vertical velocity in midlatitude regions such as the United States and Europe/east Asia. (The change in vertical velocity profile in these regions, not shown here, is near zero.) Instead, in a domain-averaged sense horizontal heat advection near the surface increases and counteracts the diabatic heating. A similar strengthening of the equatorward and eastward surface winds as a result of diabatic heating input in the midlatitudes was proposed by *Held* [1983] and found by *Coakley and Cess* [1985], *Lofgren* [1995a, 1995b], and *Chen and Ramaswamy* [1995].

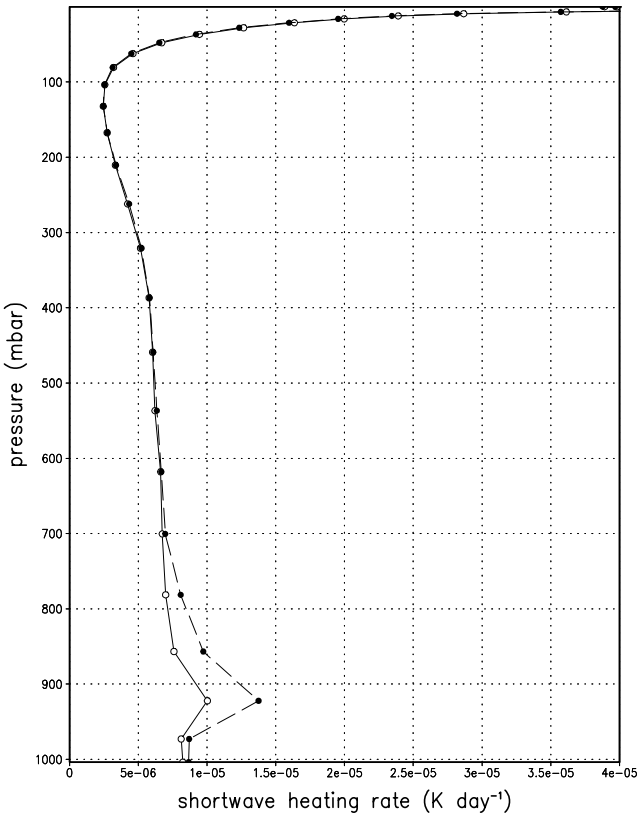

Figure 5. Global mean JJA mean SW heating rate profile for the control (solid line) and the perturbation (dotted line).

Table 2. Significance of Difference Between 12-Year Mean Control and 6-Year Mean of Perturbation for JJA Warming Regions[a]

	Global Mean	United States	Europe/East Asia	North Africa
		JJA Mean T SFC (Land)		
Control, K	293.86	298.14	196.81	302.70
Weighted SD control, K	1.49	4.26	2.56	2.16
Perturbation, K	295.10	300.46	299.02	303.38
Weighted SD perturbation, K	1.06	3.19	1.96	1.56
Weighted mean T value	3.53	2.24	3.51	1.32
Degrees of freedom	52	52	52	52
Level of confidence, %	99.95	97.5	99.95	90
		JJA Mean LOWCLD		
Control	0.18	0.038	0.025	0.0063
Weighted SD control	0.018	0.047	0.023	0.012
Perturbation	0.12	0.020	0.011	0.0035
Weighted SD perturbation	0.0072	0.018	0.0077	0.0049
Weighted mean T value	17.68	2.04	3.30	1.20
Degrees of freedom	52	52	52	52
Level of confidence, %	99.95	97.5	99.5	>75, <90

[a]Low cloud SSA = 0.99.

[16] Standard deviations, Student's *t* test values, and confidence levels of the significances for the mean JJA changes in land surface temperature and low-cloud amount are listed in Table 2, where the means are weighted by the surface area of each region. For the purposes of the *t* test, the number of degrees of freedom in each region is listed as 52 (3 months × 6 years of perturbation + 3 months × 12 years of control − 2). Note that in the weighted mean, the changes in land surface temperature and low-cloud amount are significant at above the 90% confidence level in all cases except for the low-cloud amount in North Africa. (This confidence level is not a measure of the accuracy of the model or the model input, but rather a measure of the significance of the perturbation response with respect to the model's natural internal variability.)

[17] In addition to the difference in significance levels of the means among the various regions, there are differences in signs of the changes as well. Returning to Table 1, the regions of the United States and Europe/east Asia behave similarly to the global mean, while the region of North Africa does not. In the region of the United States in JJA, the low-cloud amount decreases, while the land surface temperature increases by 2.3 K, the net SW flux at the TOA increases by 11.3 W m^{-2}, the net LW flux at the TOA decreases by 3.3 W m^{-2}, the net SW flux at the SFC increases by 5.9 W m^{-2}, and the net LW flux at the SFC decreases by 0.7 W m^{-2}. Likewise in the region of Europe/east Asia in JJA, the low-cloud amount decreases, while the land SFC temperature increases by 2.2 K, the net SW flux at the TOA increases by 9.3 W m^{-2}, the net LW flux at the TOA decreases by 5.2 W m^{-2}, the net SW flux at the SFC increases by 5.4 W m^{-2}, and the net LW flux at the SFC decreases by 2.3 W m^{-2}. Both regions exhibit a decrease in total cloud amount, also reflected in the JJA mean vertical profiles of cloud amount displayed in Figures 6 and 7. In both regions, there is also an increase in precipitable water and an increase in atmospheric stability, again reflected in a decrease in precipitation and soil moisture. In Europe/east Asia, like in the global mean, the decrease in precipitation is accompanied by a decrease in evaporation and sublimation and latent heat release from the surface, while in the United States there is a small increase in evaporation and sublimation and latent heat release due to the larger surface warming, which also reduces the soil moisture by a larger amount. Both Europe/east Asia and the United States exhibit an increase in tropospheric temperature (Figure 8).

[18] In the region of North Africa, the low-cloud amount still decreases, the land surface temperature still increases, and the precipitable water still increases, but by smaller amounts than in the other two regions. While the low clouds dissipate some, the middle and high clouds increase

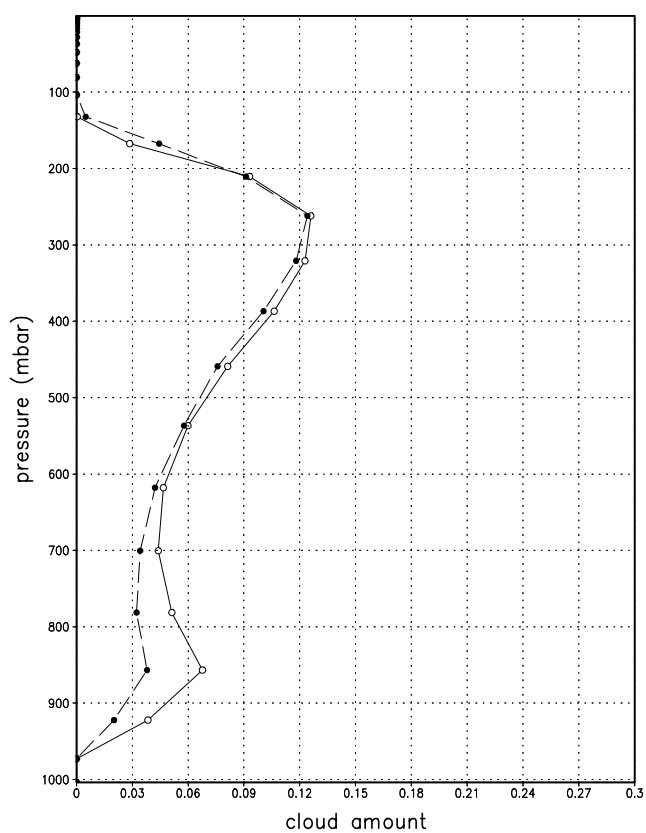

Figure 6. Same as Figure 4 but for the region of the United States.

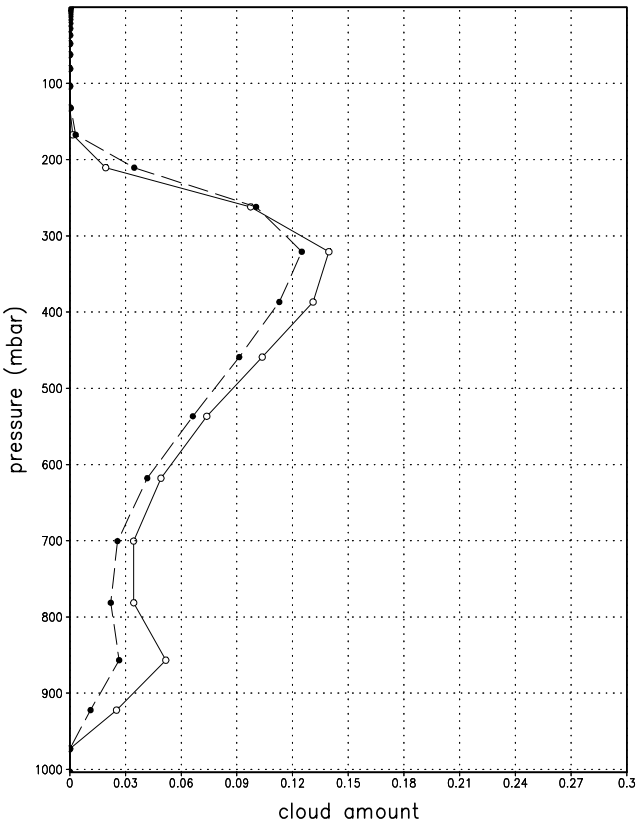

Figure 7. Same as Figure 4 but for the region of Europe/east Asia.

(Figure 9) such that the total cloud amount actually increases. In the response, the net SW flux at the TOA still increases (by 4.0 W m^{-2}) because of the solar absorption in the low-cloud layers, but to a lesser extent than in the other regions because of the increase in total cloud amount. In sharp contrast to the United States and Europe/east Asia, the increase in total cloud amount in North Africa causes the net SW flux at the SFC to decrease by 0.7 W m^{-2}. Likewise in North Africa, the LW effect of the slight warming of the surface and atmosphere is more than offset by the increase in cloudiness (or cloud frequency of occurrence) which causes the net LW flux (into the system) at the TOA to increase by 2.0 W m^{-2} (less OLR) and the net LW flux at the SFC to increase by 1.6 W m^{-2} (more emission from the atmosphere). The change in the balance at the SFC is also reflected in the precipitation, soil moisture, evaporation and sublimation, and latent heat release from the surface, which all increase in North Africa rather than decrease.

[19] Unlike the regions of the United States and Europe/east Asia, in North Africa the dominant mechanism to counteract the diabatic heating in the low-cloud layers is a decrease in atmospheric stability and an increase in convection (see Figure 10; note that downward vertical velocity is defined to be positive). The increase in upward vertical velocity causes adiabatic cooling, development of middle and high clouds (refer to Figure 9), and an increase in latent heat release within the atmosphere because of the ascent of saturated air. This distinct local, vertical balance in a region of the tropics as opposed to the midlatitudes is in good qualitative agreement with the results of *Coakley and Cess* [1985], *Lofgren* [1995a, 1995b], and *Chen and Ramaswamy* [1995]. It is interesting to note that *Andreae et al.* [2004] found a similar development of clouds above a region of cloud dissipation in the biomass burning region of the Amazon.

[20] Evidence for the differing responses of atmospheric stability in the different regions can also be seen from the change in their JJA mean temperature profiles (Figure 8). From Figure 8, the global mean, United States, and Europe/east Asia all exhibit stronger warming in the lower atmosphere than in the near surface layer below it, while North Africa does not have such a strong tendency because deep convection distributes the heating so efficiently. In all regions except for North Africa, there is an additional discontinuity between the temperature in the near surface layer and T SFC (refer to Table 1). A similar discontinuity due to interactions between the near surface layer and the surface itself, which also affect the longwave, latent heat, and sensible heat fluxes from the surface, was found by *Chen and Ramaswamy* [1995].

[21] While Figures 1–8 and Tables 1 and 2 display quantitative results, we would particularly like to emphasize their qualitative nature, as discussed in the previous paragraphs. The differing mechanisms of response between the midlatitude and equatorial continental regions are likely not very sensitive to the magnitude of the perturbation applied in this study, although the absolute values of the changes in the various quantities will vary.

[22] A schematic highlighting the differences in spatial averages of various radiative and hydrologic variables among the regions is depicted in Figure 11. Fluxes listed above the top horizontal line in Figure 11 occur at the TOA, where an upward arrow indicates a net loss from the atmosphere-surface system and a downward arrow indicates a net input to the atmosphere-surface system. In all four regions, the change in SW flux contributes a net input to the system. In the global mean, United States, and Europe/east Asia, the change in LW flux contributes a net loss from the system, while in North Africa, the change in LW flux contributes a net input. Quantities listed between the two horizontal lines in Figure 11 occur within the atmosphere, where an upward arrow indicates an absolute increase while a downward arrow indicates an absolute decrease. In all four regions, LOWCLD experiences a decrease and PREC WATER experiences an increase. In the global mean, United States, and Europe/east Asia, TOTCLD experiences a decrease, while in North Africa, TOTCLD experiences an increase. Fluxes listed below the bottom horizontal line in Figure 11 occur at the SFC, where an upward arrow indicates a net loss from the SFC while a downward arrow indicates a net gain by the SFC. For other quantities at the SFC an upward arrow indicates an absolute increase and a downward arrow indicates an absolute decrease. In all four regions, T SFC experiences an increase. In the global mean, United States, and Europe/east Asia, the change in SW flux contributes a net loss from the atmosphere and the change in LW flux contributes a net input, while in North Africa, the change in SW flux contributes a net input and the change in LW flux contributes a net loss. In the global mean, United States, and Europe/east Asia, MOISTURE and PRECIP experience decreases, while in North Africa, MOISTURE

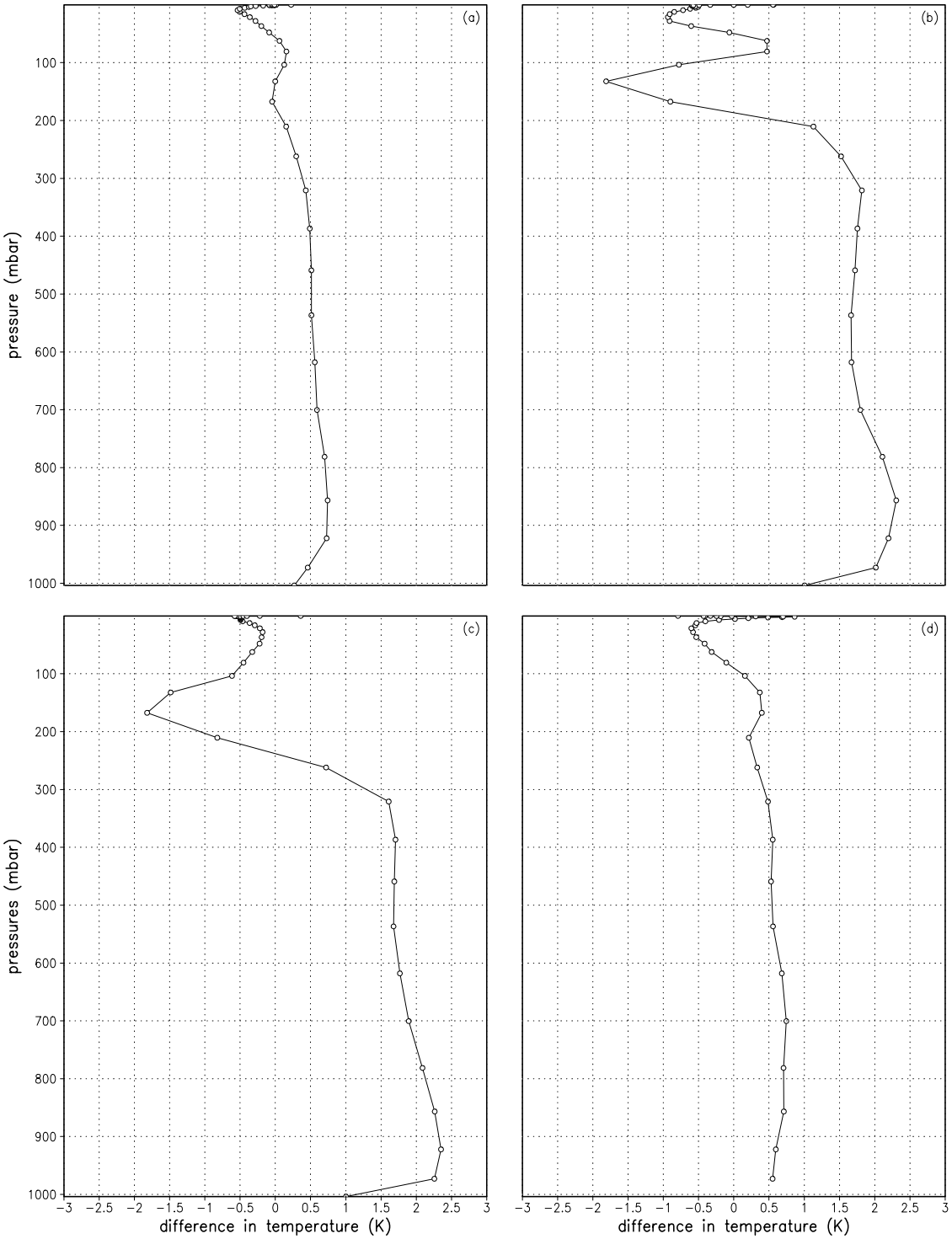

Figure 8. Difference in global mean JJA mean temperature profile between the perturbation and the control for (a) the global mean, (b) the United States, (c) Europe/east Asia, and (d) North Africa.

and PRECIP experience an increase. Other variables at the surface vary as discussed in the previous paragraphs.

[23] A global map of the precipitation changes is shown in Figure 12. In the regions of the United States and Europe/east Asia, there are areas of both increased and decreased precipitation, but the magnitude of decreased precipitation is stronger such that the area average is negative in both regions. In North Africa, the opposite is true. Note the band of strong increases and decreases in precipitation around the equator, consistent with the phenomenon of increased convection in equatorial regions such as North Africa followed by subsidence in neighboring regions.

[24] Finally we note that all of the results presented are for the months June/July/August. In order to assess the annual mean response to the idealized perturbation, other seasons need to be investigated, but it is unlikely that their

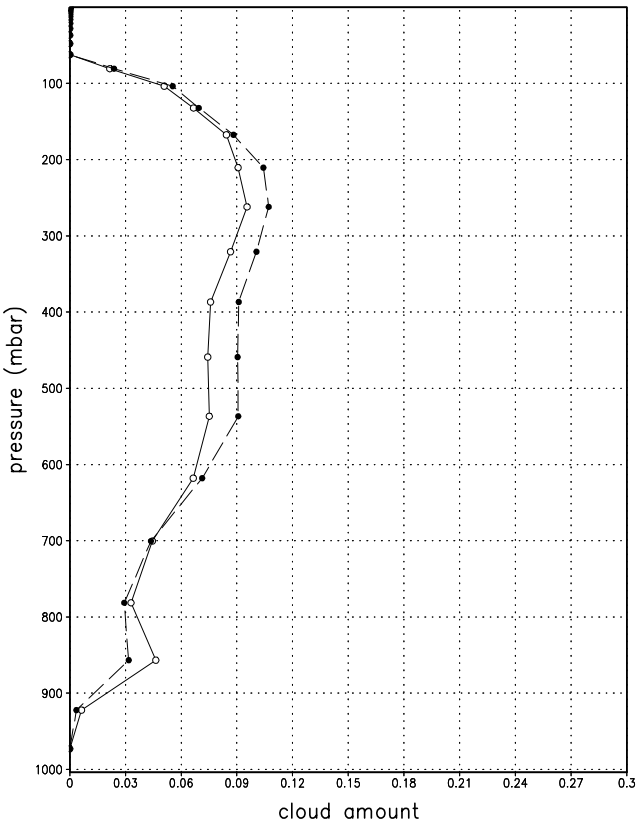

Figure 9. Same as Figure 4 but for the region of North Africa.

response will be as significant because of the larger dynamical variability during those months.

4. Comparisons With Other Climate Model Studies

[25] Here, we compare the nature of the perturbation applied here and the response with those undertaken in other recent climate model studies, that have in particular looked at the TOA and surface perturbations due to shortwave forcing agents.

[26] *Kiehl et al.* [1995] similarly increased the amount of solar absorption in clouds in the NCAR CCM2, but by a larger amount than in this study. In addition, they increased the cloud amount in order to match the observed TOA energy budget. With their larger increase in solar cloud absorption, the net SW flux at the SFC decreased, by an amount equal to the increase in SW absorption in the atmosphere (22 W m^{-2}). Despite this difference, using climatological SSTs they found a similar global decrease in precipitation and latent heat release from the SFC. However, the decrease in precipitation and latent heat release in their model is attributed to a reduction in the strength of the Hadley circulation due to the warming of the upper troposphere, leading to lower surface wind speeds. On the whole they found an increase in low clouds rather than a decrease, but they found a similar increase in cloud cover in the ITCZ and a decrease in cloud cover in the subtropics owing to the variation in middle and high clouds.

[27] The large increase in absorption leading to a reduction in net SW flux at the SFC of *Kiehl et al.* [1995] is similar to that found by *Ramanathan et al.* [2001] and *Chung et al.* [2002] from Indo-Asian haze. They found that the haze reduces the net SW flux at the SFC by 20–40 W m^{-2}, increases the SW radiation absorbed by the atmosphere by 18 W m^{-2}, heats the lower atmosphere by 0.4–0.8 K d^{-1}, and cools the land surface. Using an imposed regional forcing consisting of added atmospheric absorption from the surface up to 700 mb (unvarying with changes in cloud amount) and climatological SSTs, *Chung et al.* [2002] found that the temperature changes lead to a stabilization of the boundary layer, which is compensated by an increase in low-level convergence, convective rainfall, and latent heat release in the atmosphere. Outside of the region of the forcing, subsidence and decreased rainfall occur. Although the change in net SW flux at the SFC is similar, this local response of the surface wind and precipitation is opposite to that found by *Kiehl et al.* [1995] in their global perturbation. Note that the forcing in the *Kiehl et al.* [1995], *Ramanathan et al.* [2001], and *Chung et al.* [2002] studies is stronger at the SFC than at the TOA, whereas in the current study the opposite is true. In the work by *Kiehl et al.* [1995], the imposed increase in cloud amount reduces the forcing at the TOA, while in the work by *Chung et al.* [2002] the imposed TOA forcing inferred from observations is smaller than here.

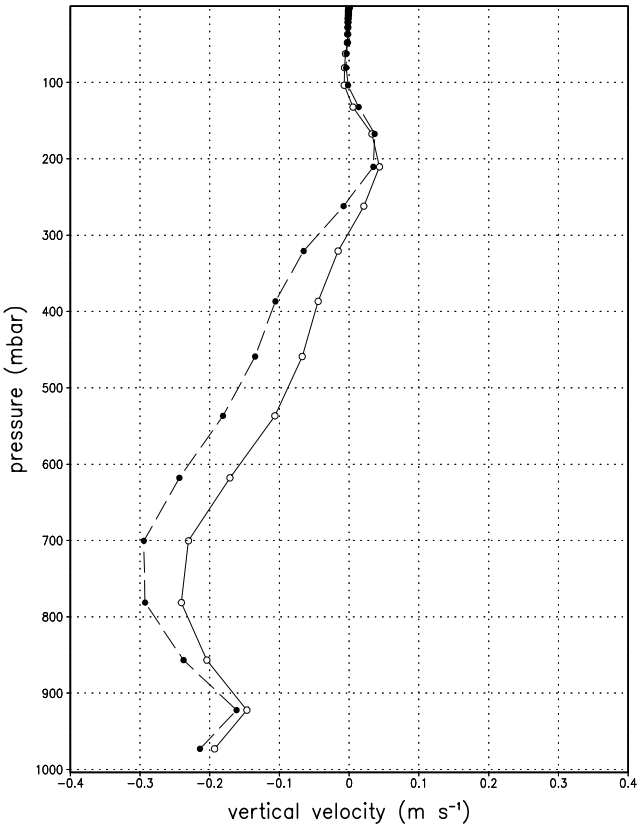

Figure 10. JJA mean vertical velocity profile for the region of North Africa for the control (solid line) and the perturbation (dotted line). Note that downward vertical velocity is defined to be positive.

	Global Mean	*United States (Land Only)*
TOA:	SW ↓ LW ↑	SW ↓ LW ↑
	TOTCLD ↓	TOTCLD ↓
	LOWCLD ↓	LOWCLD ↓
	PREC WATER ↑	PREC WATER ↑
SFC:	T ↑ SW ↓ LW ↑ SH ↓ LH ↓	T ↑ SW ↓ LW ↑ SH ↑ LH ↑
	EVAP+SUBL ↓ MOISTURE ↓ PRECIP ↓	EVAP+SUBL ↑ MOISTURE ↓ PRECIP ↓

	Europe/E. Asia (Land Only)	*N. Africa (Land Only)*
TOA:	SW ↓ LW ↑	SW ↓ LW ↓
	TOTCLD ↓	TOTCLD ↑
	LOWCLD ↓	LOWCLD ↓
	PREC WATER ↑	PREC WATER ↑
SFC:	T ↑ SW ↓ LW ↑ SH ↑ LH ↓	T ↑ SW ↑ LW ↓ SH ↓ LH ↑
	EVAP+SUBL ↓ MOISTURE ↓ PRECIP ↓	EVAP+SUBL ↑ MOISTURE ↑ PRECIP ↑

Figure 11. Schematic of the direction of change in the various variables between the perturbation and the control run for the global mean and in the three separate regions. Fluxes listed above the top horizontal line (SW and LW) occur at the TOA, where an upward arrow indicates a net loss from the atmosphere-surface system, and a downward arrow indicates a net input to the atmosphere-surface system. Quantities listed between the two horizontal lines (TOTCLD, LOWCLD, and PREC WATER) occur within the atmosphere, where an upward arrow indicates an absolute increase, and a downward arrow indicates an absolute decrease. Fluxes listed below the bottom horizontal line (SW, LW, SH, and LH) occur at the SFC, where an upward arrow indicates a net loss from the SFC, and a downward arrow indicates a net gain by the SFC. For other quantities at the SFC (T, EVAP + SUBL, MOISTURE, and PRECIP), an upward arrow indicates an absolute increase, and a downward arrow indicates an absolute decrease.

[28] Using the Reading Intermediate General Circulation Model (IGCM), *Cook and Highwood* [2004] simulated the effects of a globally uniform layer of absorbing aerosol in the lower troposphere (between 930 and 695 mb). This globally uniform pattern of forcing differs from the above mentioned studies and from the present study, as does their use of a mixed layer ocean rather than climatological SSTs. Nevertheless, the response of the surface temperature and cloud amount is similar to that of *Kiehl et al.* [1995]. When clouds were allowed to vary, they found a decrease in global annual mean surface temperature for an aerosol single-scattering albedo of 0.95, and an increase in global annual mean surface temperature for a single-scattering albedo of 0.9. For all single-scattering albedos less than 1.0, they found an increase in atmospheric temperature and stability and a reduction in the convective cloud amount. For an aerosol single-scattering albedo of 0.8, the case most similar to the present study, they found a decrease in high-cloud amount at all latitudes, an increase in middle cloud in the tropics, and a decrease in middle-cloud amount in the extratropics.

[29] The global mean decrease in low-cloud amount and increase in surface temperature that we simulate most closely resembles the results of *Hansen et al.* [1997]. Using the Wonderland GCM with a calculated ocean mixed layer temperature, *Hansen et al.* [1997] found that an absorbing aerosol layer (SSA = 0.9) in the troposphere with a nonuniform geographical distribution akin to that of sulfate and biomass burning aerosols causes a global mean warming of 0.26 K because of the decrease in low-level cloud cover. Clearly the geographical distribution of the absorption in the cloud layers is crucial in determining the response of the surface temperature.

[30] A rigorous comparison between the various modeling studies is made difficult by the fact that not only do cloud-climate interactions differ, but the way in which the TOA, atmospheric, and surface forcings are manifest, and the way in which the perturbation to the radiative balance influences the nonradiative components (e.g., sensible and latent heat fluxes) also differ from model to model. The treatment of SSTs can have a significant effect as well. With an interactive ocean, a warming of the ocean surface results in an increase in evaporation, which can lead to an increase rather than a decrease in high-cloud amount [*Cook and Highwood*, 2004] and global precipitation [*Folland et al.*, 2001; *Ramanathan et al.*, 2001]. Aerosol-cloud microphysics poses an additional factor, allowing indirect effects to compete with so-called semidirect effects, which can lead to an increase in total cloud amount in the global mean [*Lohmann and Feichter*, 2001] rather than a decrease. All of the above factors are in addition to differences in the manner in which the perturbations are applied (e.g., alteration of cloud single-scattering albedo or an imposed forcing inferred from observations), and depend on the individual GCMs' physics parameterizations (e.g., boundary layer, cloud formation and dissipation), which inhibits more of a generalization of the results from the various models.

5. Summary

[31] Using GFDL's SKYHI general circulation model, we have simulated the response of cloud amount, surface temperature, precipitation, and surface fluxes to absorption

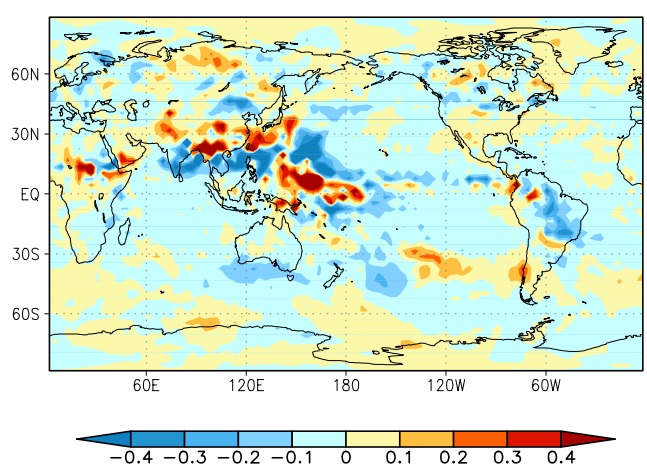

Figure 12. Change in JJA mean precipitation (mm d^{-1}) between the 6-year perturbation and the 12-year control.

of solar radiation in low-cloud layers during the northern summer season due to the presence of continental type absorbing aerosols. To simulate the effect of the presence of continental type absorbing aerosols, the single-scattering albedo of all low clouds was reduced from its nominal value near 1.0 to 0.99 for all wavelengths between 0.2 and 1.2 μm. This has been an idealized experiment, designed to flush out the fundamental manner of response over different continental regions when a similar solar radiative perturbation is applied to all of them.

[32] We found that globally, the reduction in low-cloud single-scattering albedo causes a warming of the surface, stabilization of the lower troposphere, and a reduction in the hydrological cycle (precipitation, soil moisture, evaporation and sublimation, and latent heat flux from the surface). Surface warming and atmospheric stabilization were obtained in a similar radiative convective model experiment where cloud amount was held constant and horizontal dynamics were absent, indicating that the global mean response of the surface and atmosphere is robust even under changes in cloud amount and dynamics. However, while it might be a natural inclination to compare the RCM and GCM, since the overall tendencies of response are similar, in fact one must keep in mind that the mechanisms of surface warming and atmospheric stabilization are substantially different in the GCM. While in the RCM there is efficient vertical diffusion of the local diabatic heating (as in North Africa in these GCM simulations), in the GCM the diabatic heating leads to a global decrease in low-cloud amount, allowing more solar radiation to reach the surface, and to a regional increase in horizontal heat advection.

[33] We find that, in the global mean, the perturbation to the net shortwave flux is quite evenly split between the surface and atmosphere in the new equilibrium state. While the decrease in low-cloud amount acts to put extra shortwave flux into the surface, there is extra absorption of shortwave flux in the atmosphere below 700 mb as well, owing to the decreased low-cloud single-scattering albedo and the increase in atmospheric water vapor. Therefore the aerosol-cloud interaction involving low clouds consists of a significant perturbation of shortwave atmospheric absorption (increase of flux convergence), as well as a forcing at the TOA and SFC.

[34] While the regional changes in surface temperature and low-cloud amount are consistent with the global mean, we found that the change in shortwave flux at the surface and response of the hydrological cycle vary from region to region. Considering continental scales, while the midlatitude regions of the United States and Europe/east Asia behave similarly to the global mean, the tropical region of North Africa exhibits a different surface energy balance. Unlike the regions of the United States and Europe/east Asia, in North Africa the diabatic heating in the low clouds leads to an increase in convection, a decrease in stability, and an increase in middle- and high-level clouds. The increase in middle and high clouds leads to a reduction in shortwave flux to the surface and an increase in precipitation, soil moisture, evaporation and sublimation, and latent heat flux from the surface. Such a distinctive balance in the tropics was also found by *Chen and Ramaswamy* [1995], *Ramanathan et al.* [2001], and *Chung et al.* [2002], although the direction of change in surface temperature and surface winds varied, depending on the strength of the perturbation.

[35] A survey of modeling studies reveals the commonality that absorption by water clouds, whether with absorbing aerosols present externally or internally within drops, effectively alters the cloud layer single-scattering albedo and leads to a redistribution of SW radiation, wherein less reaches the surface and more is absorbed in the layers where clouds are present. This in turn leads to a warming of the free troposphere and a stabilization of the atmosphere. Surface temperature and surface energy and moisture balance, however, are affected by boundary layer processes and thus can be quantitatively different in different models. Also, the manner in which the diabatic warming input in any continental region translates into temperature increases versus increases in vertical velocity can vary between the tropics and midlatitudes, and this response can also be of differing magnitudes in different models. There can be considerable spatial heterogeneity as well, for example, subcontinental-scale changes can be quite different from continental-scale averages.

[36] The results presented lend further support for the importance of taking into consideration the aerosol absorption effects on clouds in the lower troposphere and the ensuing effects on climate, including so-called semidirect effects. However, the global mean response of the climate is not an indication of the regional response, and a full understanding of the response of the climate to such a perturbation can only be gained by looking at the regional scale, and investigating both radiative and hydrologic budgets, where the mechanisms and effects prevailing in the tropical and midlatitude domains can be quite different from one another. Even when the radiative pattern of solar absorption in the atmosphere is well understood, as is the case in our idealized simulations, the responses of different regions may not follow in a similar manner. Our main conclusion is that even for an idealized uniform aerosol distribution, the response is not similar everywhere, not even qualitatively. Any departure from these globally uniform, idealized conditions could yield even more differences.

[37] **Acknowledgments.** The authors thank D. Schwarzkopf for assistance with the GCM, S. Ramachandran for helpful discussions, and two anonymous reviewers for their comments. C.E. acknowledges financial support provided by Israel Science Foundation grant 1315/04.

References

Ackerman, A. S., and O. B. Toon (1996), Unrealistic dessication of marine stratocumulus clouds by enhanced solar absorption, *Nature*, *380*, 512–515.

Ackerman, A. S., O. B. Toon, D. E. Stevens, A. J. Heymsfield, V. Ramanathan, and E. J. Welton (2000), Reduction of tropical cloudiness by soot, *Science*, *288*, 1042–1047.

Albrecht, B. (1989), Aerosols, cloud microphysics, and fractional cloudiness, *Science*, *245*, 1227–1230.

Andreae, M. O., D. Rosenfeld, P. Artaxo, A. A. Costa, G. P. Frank, K. M. Longo, and M. A. F. Silva-Dias (2004), Smoking rain clouds over the Amazon, *Science*, *303*, 1337–1342.

Chen, C.-T., and V. Ramaswamy (1995), Parameterization of the solar radiative characteristics of low clouds and studies with a general circulation model, *J. Geophys. Res.*, *100*(D6), 11,611–11,622.

Chung, C. E., V. Ramanathan, and J. T. Kiehl (2002), Effects of south Asian absorbing haze on the northeast monsoon and surface-air heat exchange, *J. Clim.*, *15*, 2462–2476.

Coakley, J. A., Jr., and R. D. Cess (1985), Response of the NCAR Community Climate Model to the radiative forcing by the naturally occurring tropospheric aerosol, *J. Atmos. Sci.*, *42*, 1677–1692.

Conant, W. C., A. Nenes, and J. H. Seinfeld (2002), Black carbon radiative heating effects on cloud microphysics and implications for the aerosol indirect effect: 1. Extended Köhler theory, *J. Geophys. Res.*, *107*(D21), 4604, doi:10.1029/2002JD002094.

Cook, J., and E. J. Highwood (2004), Climate response to tropospheric absorbing aerosols in an intermediate general-circulation model, *Q. J. R. Meteorol. Soc.*, *130*, 175–191.

Cooke, W. F., V. Ramaswamy, and P. Kasibhatla (2002), A general circulation model study of the global carbonaceous aerosol distribution, *J. Geophys. Res.*, *107*(D16), 4279, doi:10.1029/2001JD001274.

Erlick, C., and V. Ramaswamy (2003), Sensitivity of the atmospheric lapse rate to solar cloud absorption in a radiative-convective model, *J. Geophys. Res.*, *108*(D16), 4522, doi:10.1029/2002JD002966.

Erlick, C., L. M. Russell, and V. Ramaswamy (2001), A microphysics-based investigation of the radiative effects of aerosol-cloud interactions for two MAST experiment case studies, *J. Geophys. Res.*, *106*(D1), 1249–1269.

Folland, C. K., et al. (2001), Observed climate variability and change, in *Climate Change 2001: The Scientific Basis*, edited by J. T. Houghton et al., pp. 99–181, Cambridge Univ. Press, New York.

Freidenreich, S. M., and V. Ramaswamy (1999), A new multiple band solar radiative parameterization for general circulation models, *J. Geophys. Res.*, *104*(D24), 31,389–31,409.

Hamilton, K. P., R. J. Wilson, J. D. Mahlman, and L. Umscheid (1995), Climatology of the SKYHI troposphere-stratosphere-mesosphere general circulation model, *J. Atmos. Sci.*, *52*, 5–43.

Hansen, J., M. Sato, and R. Ruedy (1997), Radiative forcing and climate response, *J. Geophys. Res.*, *102*(D6), 6831–6864.

Hansen, J., M. Sato, R. Ruedy, A. Lacis, and V. Oinas (2000), Global warming in the twenty-first century: An alternative scenario, *Proc. Natl. Acad. Sci. U. S. A.*, *97*(18), 9875–9880.

Held, I. M. (1983), Stationary and quasi-stationary eddies in the extratropical troposphere: Theory, in *Large Scale Dynamic Processes in the Atmosphere*, edited by B. J. Hoskin and R. P. Pearce, pp. 127–168, Elsevier, New York.

Johnson, B. T., K. P. Shine, and P. M. Forster (2004), The semi-direct aerosol effect: Impact of absorbing aerosols on marine stratocumulus, *Q. J. R. Meteorol. Soc.*, *130*, 1407–1422.

Kiehl, J. T., J. J. Hack, M. H. Zhang, and R. D. Cess (1995), Sensitivity of a GCM to enhanced shortwave cloud absorption, *J. Clim.*, *8*, 2200–2212.

Liousse, C., J. E. Penner, C. Chuang, J. J. Walton, H. Eddleman, and H. Cachier (1996), A global three-dimensional model study of carbonaceous aerosols, *J. Geophys. Res.*, *101*(D14), 19,411–19,432.

Lofgren, B. M. (1995a), Sensitivity of land ocean circulations, precipitation, and soil-moisture to perturbed land-surface albedo, *J. Clim.*, *8*, 2521–2542.

Lofgren, B. M. (1995b), Surface albedo climate feedback simulated using 2-way coupling, *J. Clim.*, *8*, 2543–2562.

Lohmann, U., and J. Feichter (2001), Can the direct and semi-direct aerosol effect compete with the indirect effect on a global scale?, *Geophys. Res. Lett.*, *28*(1), 159–161.

Lohmann, U., J. Feichter, J. E. Penner, and W. R. Leaitch (2000), Indirect effect of sulfate and carbonaceous aerosols: A mechanistic treatment, *J. Geophys. Res.*, *105*(D10), 12,193–12,206.

Peixoto, J. P., and A. H. Oort (1992), *Physics of Climate*, 520 pp., Am. Inst. of Phys., New York.

Pincus, R., and H. B. Baker (1994), Effect of precipitation on the albedo susceptibility of clouds in the marine boundary-layer, *Nature*, *372*, 2250–2252.

Ramachandran, S., V. Ramaswamy, G. L. Stenchikov, and A. Robock (2000), Radiative impact of Mount Pinatubo volcanic eruption: Lower stratospheric response, *J. Geophys. Res.*, *105*(D19), 24,409–24,429.

Ramanathan, V., et al. (2001), Indian Ocean Experiment: An integrated analysis of the climate forcing and effects of the great Indo-Asian haze, *J. Geophys. Res.*, *106*(D22), 28,371–28,398.

Ramaswamy, V., and M. D. Schwarzkopf (2002), Effects of ozone and well-mixed gases on annual-mean stratospheric temperature trends, *Geophys. Res. Lett.*, *29*(22), 2064, doi:10.1029/2002GL015141.

Ramaswamy, V., O. Boucher, J. Haigh, D. Hauglustaine, J. Haywood, G. Myhre, T. Nakajima, G. Y. Shi, and S. Solomon (2001), Radiative forcing of climate change, in *Climate Change 2001: The Scientific Basis*, edited by J. T. Houghton et al., pp. 349–416, Cambridge Univ. Press, New York.

Rosenfeld, D. (1999), TRMM observed first direct evidence of smoke from forest fires inhibiting rainfall, *Geophys. Res. Lett.*, *26*(20), 3105–3108.

Rosenfeld, D. (2000), Suppression of rain and snow by urban and industrial air pollution, *Science*, *287*, 1793–1796.

Schwarzkopf, M. D., and S. B. Fels (1991), The simplified exchange method revisited: An accurate, rapid method for computation of infrared cooling rates and fluxes, *J. Geophys. Res.*, *96*(D5), 9075–9096.

Schwarzkopf, M. D., and V. Ramaswamy (1999), Radiative effects of CH_4, N_2O, halocarbons and the foreign-broadened H_2O continuum: A GCM experiment, *J. Geophys. Res.*, *104*(D8), 9467–9488.

Slingo, A. (1989), A GCM parameterization for the shortwave radiative properties of water clouds, *J. Atmos. Sci.*, *46*, 1419–1427.

Twomey, S. A. (1991), Aerosols, clouds, and radiation, *Atmos. Environ., Part A*, *25*, 2435–2442.

Wetherald, R. T., and S. Manabe (1988), Cloud feedback processes in a general circulation model, *J. Atmos. Sci.*, *45*, 1397–1415.

C. Erlick, Department of Atmospheric Sciences, Hebrew University of Jerusalem, Jerusalem 91904, Israel. (caryn@vms.huji.ac.il)

V. Ramaswamy, Geophysical Fluid Dynamics Laboratory, Princeton University, Princeton, NJ 08452, USA.

L. M. Russell, Scripps Institution of Oceanography, University of California, San Diego, CA 92093-0221, USA.